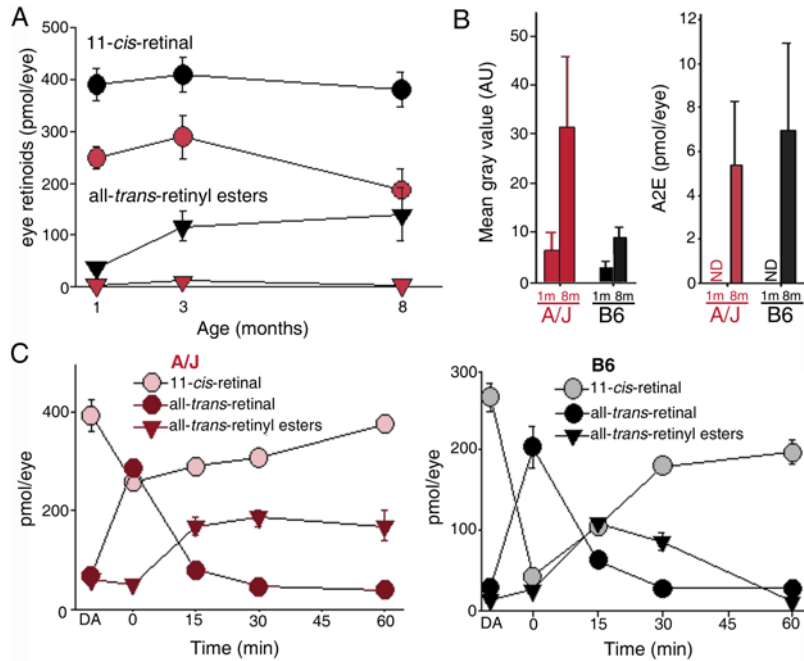


Supplemental material

Inflammatory priming predisposes to age-related retinal degeneration in mice

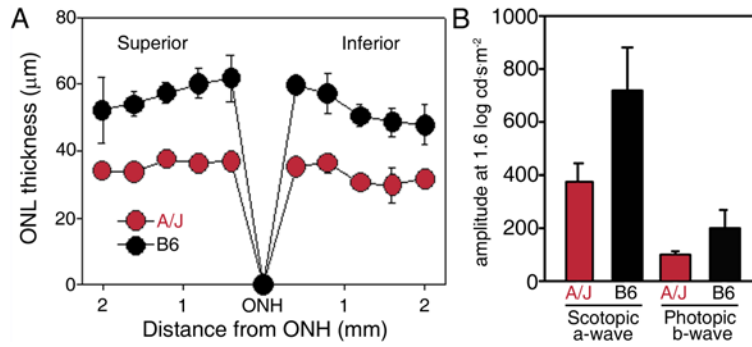
Debarshi Mustafi, Tadao Maeda, Hideo Kohno, Joseph H. Nadeau, and Krzysztof Palczewski

Supplemental Figure 1



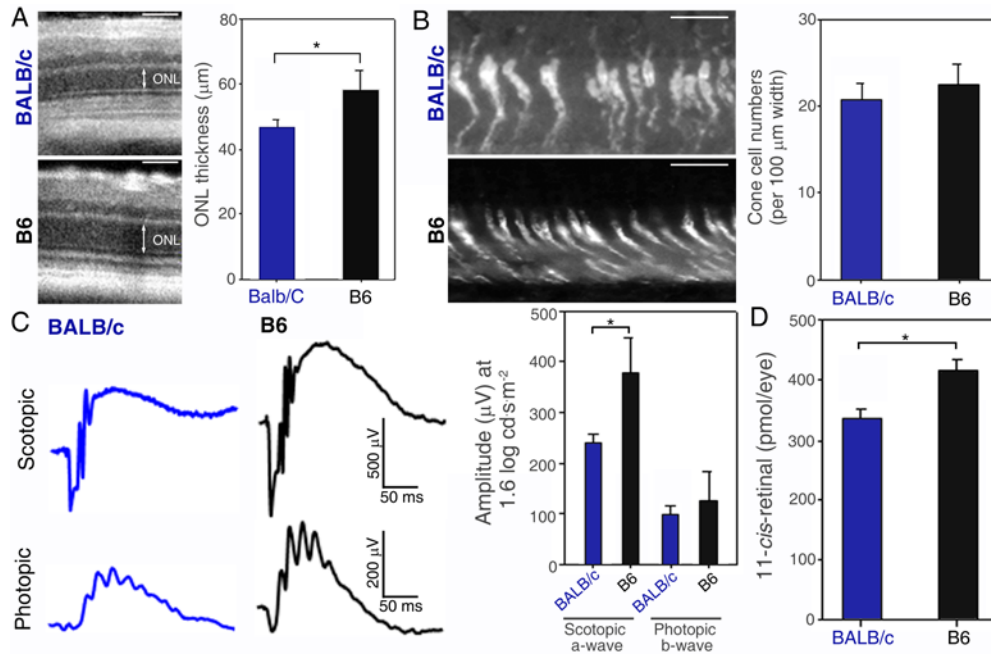
A/J and B6 mouse eyes exhibit different retinoid content profiles. **(A)** Normal-phase HPLC separation of nonpolar retinoids from retinal homogenates of 1-, 3-, and 8-month-old A/J and B6 mouse eyes showed decreased levels of both 11-*cis*-retinal (top) and all-*trans*-retinyl esters (bottom) in A/J (red symbols) relative to B6 (black symbols) mice. These differences were most pronounced at 8-months of age ($n > 8$). **(B)** Fundus autofluorescence (AF) was measured by SLO (485 nm excitation; emission filter, 500–700 nm) at 1- and 8-months of age. The intensities of AF plotted as mean gray values revealed a 4-fold increase in A/J mice at 8-months of age as compared to 1-month of age whereas only a mild age-related increase of AF intensity was noted in B6 mice. A2E, one of the main fluorophores in the retina, was extracted from 1- and 8-month-old mouse eyes and quantified by normal phase HPLC. Amounts of A2E increased with age in both A/J and B6 mice but did not correlate with the degree of fundus AF. **(C)** In both A/J (left panel) and B6 (right panel) mice, the retinoid cycle was functional at 1.5-months of age and the 11-*cis*-retinal regeneration ratio in A/J mice after a light stimulus ($10000 \text{ cd} \cdot \text{m}^{-2}$, less than 2 ms) was 2-fold higher than in B6 mice. This is consistent with the increased expression of RPE65 in A/J mice. **B, C:** $n > 3$ at each time point. Bars indicate standard deviation (SD) in all panels.

Supplemental Figure 2



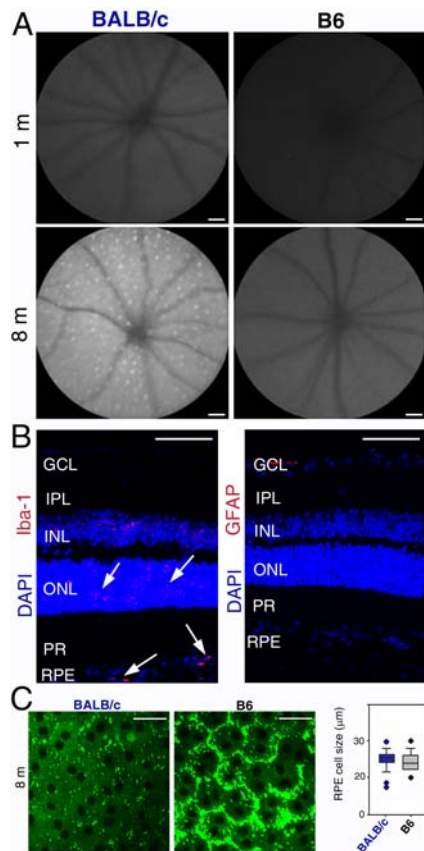
Age-related degenerative changes in eyes of A/J mice are independent of lighting conditions. (A) Thicknesses of the ONL plotted as a function of distance from the optic nerve head (ONH; in mm) in retinas of 8-month-old A/J (red circles) and B6 (black circles) mice maintained in the dark illustrate that age-related changes in A/J mouse retina does not depend on exposure to light ($n > 4$). (B) Plots of functional a-wave amplitudes under scotopic condition and b-wave amplitudes under photopic conditions obtained from A/J and B6 mice at 8-months of age are shown. ERG responses were attenuated in A/J relative to B6 mice under both scotopic and photopic conditions ($n > 4$, $P < 0.001$). Bars indicate SDs.

Supplemental Figure 3



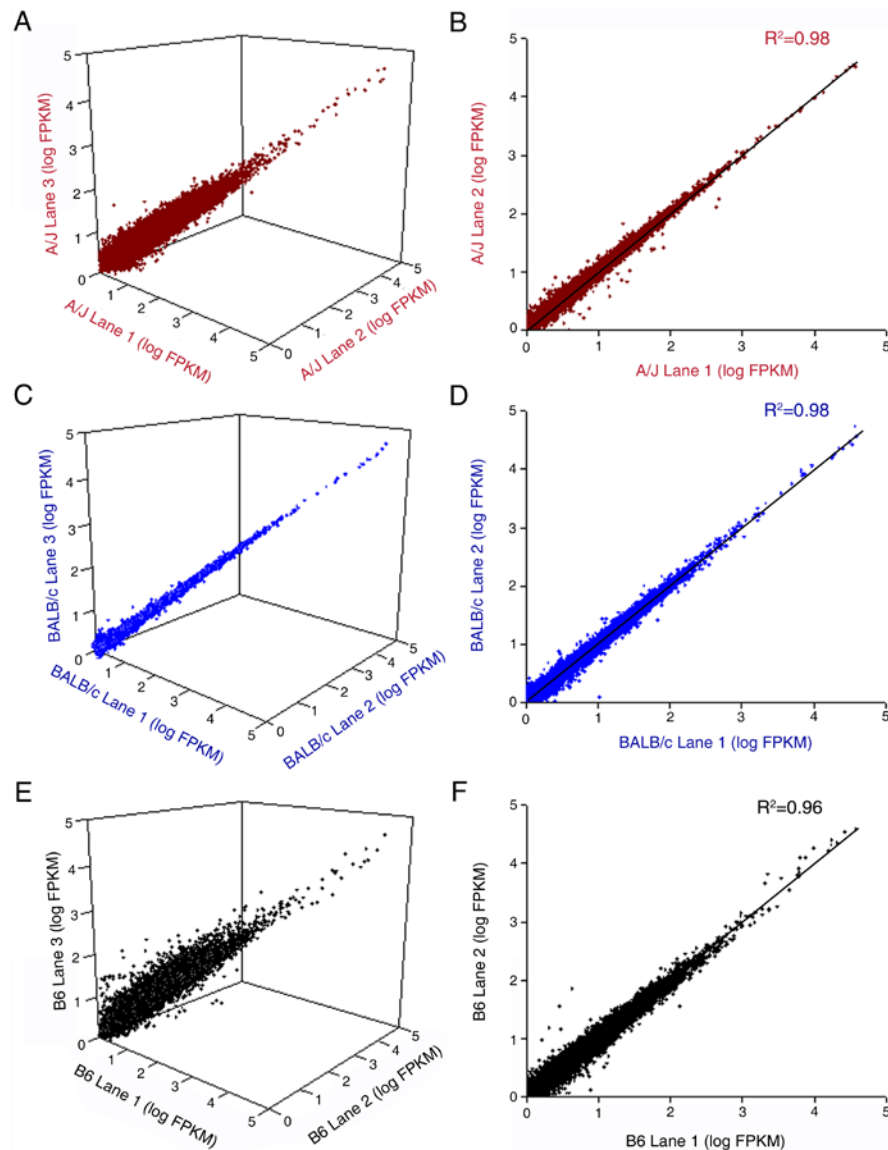
Mild progression of age-dependent retinal dysfunction in BALB/c mice. **(A)** In vivo SD-OCT imaging of retinal cross-sections from BALB/c and B6 mice reveals a mild decrease in outer nuclear layer (ONL) thickness in BALB/c as compared to B6 mice at 8-months of age. **(B)** Cone cell sheaths in retinal cross sections were imaged by PNA staining (left panels) and numbers of cone cells were counted in both the superior and inferior retina over a 100 μm range located 500 μm away from ONH and the average number was plotted (right panel). Numbers of cone cells were comparable in BALB/c mice and B6 mice at 8-months of age. **(C)** Representative ERG responses at 1.6 log cd·s·m⁻² are shown in the left panels and functional a-wave amplitudes under scotopic conditions and b-wave amplitudes under photopic conditions obtained from BALB/c and B6 mice at 8-months of age were plotted (right panel). ERG responses were attenuated in BALB/c relative to B6 mice under scotopic conditions (P<0.001) whereas amplitudes were comparable between the two strains under photopic conditions, consistent with the results illustrated in panels **A** and **B**. **(D)** Amounts of the visual chromophore, 11-cis-retinal, in the eye, which are comparable to those of visual pigments, were quantified by HPLC at 8-months of age. Amounts of 11-cis-retinal in the BALB/c mouse eye were 80% of those found in the B6 mouse eye. Three to four animals were evaluated for each experimental condition. ONL, outer nuclear layer. Scale bars are 40 μm in panel **A** and 20 μm in panel **B**. Bars indicate SDs in all panels. Asterisks indicate statistically significant differences.

Supplemental Figure 4



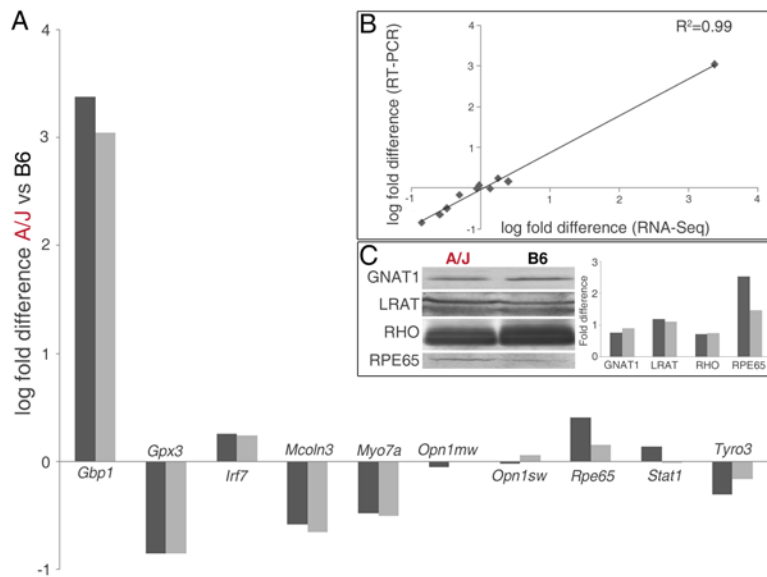
Increased autofluorescence in BALB/c mice with age occurs without obvious pathological changes in the RPE. (A) Representative SLO autofluorescent images are shown of BALB/c and B6 mouse outer retina (485 nm excitation; emission filter, 500–700 nm). BALB/c mice exhibited age-related (1– to 8–months) increased autofluorescence and punctate white dots not seen in B6 mice ($n > 3$). (B) Compared to B6 mouse retina, 8-month-old BALB/c mouse retina featured mild cellular infiltration resulting from inflammatory and immune cell activation evidenced by Iba-1 staining (activated microglia cells) and GFAP staining (activated Müller glial cells and astrocytes). Slight staining of Iba-1, indicated by arrows, was not recognized by the GFAP stain. (C) The size and morphology of RPE cells from 8-month-old BALB/c and B6 mice were imaged by TPM. No obvious pathological changes were detected in the RPE of BALB/c mice and RPE cell sizes were comparable to those of B6 mice ($n > 50$). Labeled layers of the retina are: GCL, ganglion cell layer; INL, inner nuclear layer; ONL, outer nuclear layer; IS, inner segment; OS, outer segment; RPE, retinal pigmented epithelium. Scale bars are 40 μm in panel A, 50 μm in panel B, and 20 μm in panel C. Bars indicate SDs in panel C.

Supplemental Figure 5



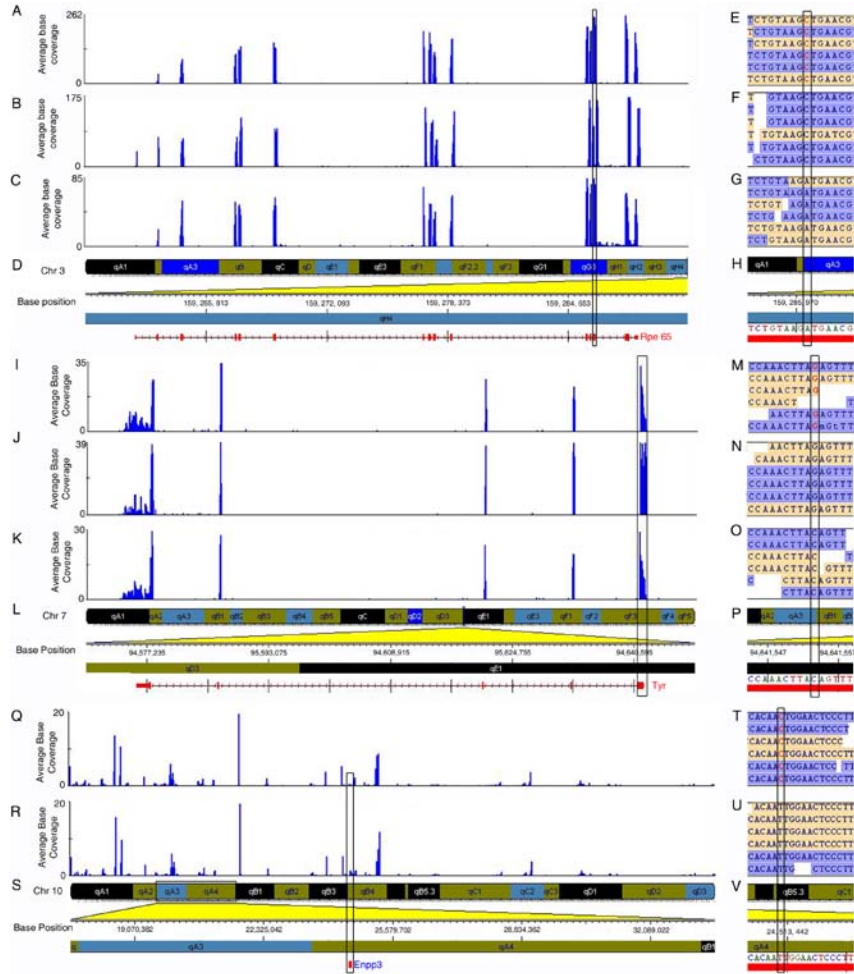
RNA-Seq of biological replicates of 1-month old eye tissue from A/J, BALB/c and B6 mice reveals high reproducibility of individual background runs. For mice of each genetic background (A/J, BALB/c, and B6), three biological replicate eye samples were run on individual lanes of an Illumina Genome Analyzer IIx. (A) A plot of the three biological replicate runs for A/J mouse eyes showed little variability. (B) Most reads from biological replicate runs fell along the line representing equal expression, with a high correlation coefficient of 0.98. Similarly, a plot of the three biological replicate runs for BALB/c mouse eyes, (C) and (D), and B6 mouse eyes, (E) and (F), also displayed the same equal expression with correlation coefficients of 0.98 and 0.96, respectively. The overall strong correlation of biological replicate runs indicates that any differential expression between genetic backgrounds did not result from sequencing errors. Moreover, use of three biological replicates for each genetic background allowed statistical calculations to remove outlier differences.

Supplemental Figure 6



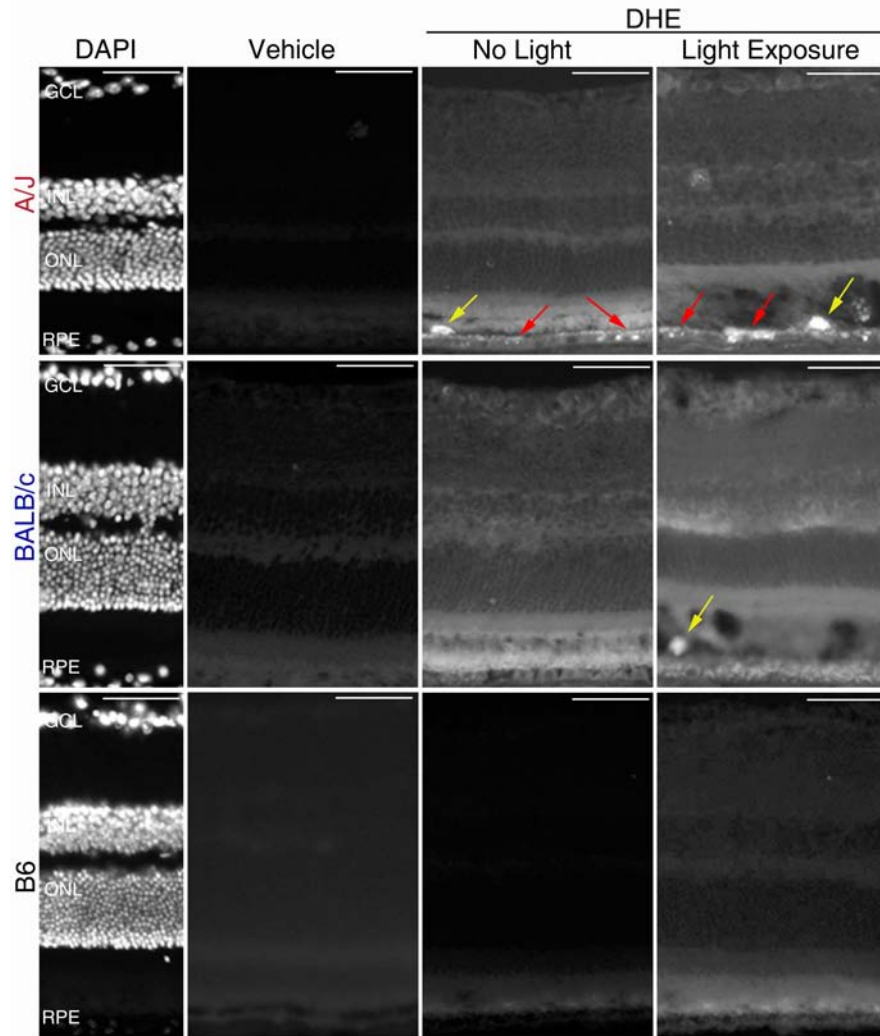
RNA-Seq data are verified by RT-PCR and immunoblotting. (A) RT-PCR validates the differential expression profile detected by RNA-Seq with different probes for genes exhibiting either high or low differential expression compared to those with virtually equal expression in eyes of A/J and B6 mice. Dark gray bars represent the RNA-Seq values and light gray bars, the RT-PCR values. (B) The correlation between the RT-PCR and RNA-Seq findings was extremely high ($R^2=0.99$). (C) RNA-Seq changes also predicted selected protein level changes assessed by immunoblots of the common visual cycle proteins GNAT1, LRAT, RHO and RPE65. Protein separation was performed on 12% SDS-PAGE gels. Immunoblotting (Immobilon-P polyvinylidenedifluoride; Millipore) was carried out according to standard protocols. Alkaline phosphatase-conjugated goat anti-mouse IgG or goat anti-rabbit IgG (Promega) were used as secondary antibodies. Protein bands were visualized with 5-bromo-4-chloro-3-indolyl phosphate/nitro blue tetrazolium color development substrate (Promega). Dark gray bars represent the immunoblot intensities and light gray bars the RNA-Seq transcript level changes. Anti-GNAT1, LRAT and RPE65 mAbs were generated in our lab as previously described (1-3).

Supplemental Figure 7



Key SNPs are identified by RNA-seq. In albino A/J and BALB/c mice there is a missense mutation in *RPE65* at amino acid 450 that contributes differentially to light-induced retinal damage. We noted increased amounts in (A) A/J and (B) BALB/c mice as compared to (C) B6 mice of (D) the *Rpe65* message and also found that the nucleotide change in (E) A/J and (F) BALB/c mice was not evident in (G) B6 mice or the (H) reference assembly that should give rise to this altered protein product. The *Tyr* transcript is known to be transcribed at similar levels in A/J, BALB/c, and B6 mice, but a single mutation at nucleotide position 308 that causes a missense mutation at amino acid 103 (cysteine to serine) abolishes pigment production in albino mice. We found similar levels in (I) A/J, (J) BALB/c, and (K) B6 mice of (L) this *Tyr* message. We also observed a mutation at nucleotide position 308 in (M) A/J and (N) BALB/c mice that was not evident in (O) B6 mice or (P) the reference assembly that would give rise to the missense mutation noted. Our expanded analysis to a QTL region in chromosome 10 revealed differential expression of *Enpp3* and a SNP corresponding to a missense mutation. Compared to (Q) A/J mice, there was greater expression in (R) B6 mice of (S) *Enpp3*. Examination of this gene revealed a SNP at position 24,513,440 in (T) A/J mice that gives rise to a missense mutation that was not evident in (U) B6 mice or (V) the reference assembly.

Supplemental Figure 8



In vivo ROS generation is detected in the RPE of aged A/J mice. Eight-month-old A/J, BALB/c and B6 mice were dark-adapted overnight and treated with the ROS probe, DHE, by intraperitoneal injection 1 h prior to 5,000 lux light exposure for 30 min. DMSO was used as the vehicle control (Vehicle). Dark-adapted mice unexposed to experimental light were included for the DHE probe treatment as well (No Light). Retinas were harvested 3 h after illumination. ROS signals were captured with a fluorescence microscope under identical exposure conditions. DAPI staining revealed a representative orientation of nuclear layers in retinal cross sections. ROS signals were observed in the RPE of A/J mouse retina irrespective of light exposure (red arrows) and from infiltrated inflammatory cells (yellow arrows) located above the RPE cell layer ($n > 5$). ROS signals from inflammatory cells also were noted in light-exposed BALB/c mice whereas non-specific background signals were seen in both BALB/c and B6 mouse retina ($n > 5$). Labeled layers of the retina are as follows: GCL, ganglion cell layer; INL, inner nuclear layer; ONL, outer nuclear layer; RPE, retinal pigmented epithelium. Scale bars are 50 μm .

Supplemental Table 1. GoTerm breakdown of transcript reads across different RNA–Seq experiments with from 1-month-old A/J, BALB/c and B6 mice whole eye tissue.

Go Term	A/J Eye	BALB/c Eye	B6 Eye
Autophagy	28 (0.22)	27 (0.21)	28 (0.22)
Binding activity	1,077 (8.54)	1,055 (8.38)	1,083 (8.44)
Biogenesis	94 (0.75)	95 (0.75)	96 (0.75)
Catalytic activity	178 (1.41)	181 (1.44)	182 (1.42)
Cell adhesion	306 (2.43)	307 (2.44)	327 (2.55)
Cell cycle	337 (2.67)	321 (2.55)	326 (2.54)
Cell death	185 (1.47)	185 (1.47)	189 (1.47)
Cytoskeleton organization	172 (1.36)	170 (1.35)	173 (1.35)
Developmental process	185 (1.47)	192 (1.53)	196 (1.53)
DNA repair	144 (1.14)	143 (1.14)	144 (1.12)
Homeostatic process	113 (0.90)	114 (0.91)	116 (0.90)
Metabolic process	1,886 (14.96)	1,862 (14.79)	1,897 (14.78)
No term	2,456 (19.48)	2,483 (19.72)	2,510 (19.58)
Protein folding	97 (0.77)	98 (0.78)	99 (0.77)
Protein modification	456 (3.62)	456 (3.62)	464 (3.62)
Regulatory process	263 (2.09)	261 (2.07)	263 (2.05)
RNA processing	362 (2.87)	363 (2.88)	364 (2.84)
Signal transduction	1,254 (9.95)	1,256 (9.98)	1,297 (10.11)
Structural molecule activity	103 (0.82)	103 (0.82)	106 (0.83)
System process	89 (0.71)	85 (0.68)	82 (0.64)
Transcription	1,213 (9.62)	1,215 (9.65)	1,230 (9.59)
Translation	268 (2.13)	281 (2.23)	283 (2.21)
Transport	1,340 (10.63)	1,336 (10.61)	1,374 (10.71)
Total transcripts (> 1 FPKM)	12,606	12,589	12,832

All transcripts detected at a level of 1 FPKM (average of three biological replicate runs) in A/J, BALB/c, and B6 whole eye samples were subjected to GoTerm categorization with Amigo v1.8. Numbers in parenthesis indicate the percentage of transcripts that fell into the listed category.

Supplemental Table 2. Differential expression profile of genes in the A/J and B6 mouse eye and SNP analysis of differentially expressed genes. A total of 332 genes were differentially expressed by at least 2 –fold ($p < 0.05$) in A/J and B6 mouse eyes. The breakdown of fold differences is listed. SNPs in these sets of genes are also listed with coding region SNPs classified as synonymous, non-synonymous or untranslated region (UTR). UTR SNPs are further identified as either 3' or 5' SNPs. Of the 393 coding SNPs identified, 75 were not found in the dbSNP database encompassing 37 different genes.

	A/J Eye	B6 Eye
Higher in expression by >2 fold	117	215
>5–fold	27	33
3–5–fold	25	60
2–3–fold	65	132
Genes with SNPs	47	58
Total SNPs	232	229
Coding Region SNPs	182	211
Synonymous SNPs	66	62
Non-Synonymous SNPs	40	23
UTR SNPs	76	126*
3' UTR SNPs	71	122
5' UTR SNPs	5	3

*One of these UTR SNPs lies at a predicted splice site.

SNP detection and analysis was done with the GenomeStudio RNA Sequencing Module (Illumina). Allelic base calls for A/J and BALB/c mice were analyzed for those that differed (Call type: Diff) from the reference base (C57BL/6). Only different base calls that were common to all three different biological replicate sample lanes were considered as SNPs for further analysis. SNPs were analyzed to see if they fell within exon boundaries of genes of interest. Coding region SNPs were further characterized as either synonymous, non –synonymous, or UTR based on SNPs noted in NCBI dbSNP Build 128 for *mus musculus*. If SNPs were not found in the database, they were manually examined with the University of California Santa Cruz mouse genome assembly (mm9).

Supplemental Table 3. Transcript reads (FPKM) of selected genes from A/J, BALB/c, and B6 mice as well as from Long –Evans rat and Nile rat eyes. The three inbred mouse models were compared to two different rodent species with varying photoreceptor populations: the nocturnal Long –Evans rat, which possesses a large rod population and the diurnal Nile rat, which has a large percentage of cone photoreceptors. Selected examination of photoreceptor genes revealed the relative rod dominance in the Long –Evans rat (increased *Rho* expression) and the cone dominance in the Nile rat (increased *Opn1mw* expression). Examination of selected retinal homeostasis and inflammatory genes revealed that Long –Evans and Nile rats possess retinal environments distinct from A/J mice that are most similar to B6 mice.

Rod and Cone Photoreceptor Genes

Gene	A/J	BALB/c	B6	Long–Evans rat	Nile rat
Opn1mw	54.68	44.36	62.97	36.38	162.00
Rho	4365.69	5389.12	61.62	9831.11	1918.14

Retinal Homeostasis Genes

Gene	A/J	BALB/c	B6	Long–Evans rat	Nile rat
Bmp4	17.57	15.06	10.62	11.36	8.20
Gpx3	29.6	82.90	205.55	77.18	7.00
Hspb1	62.85	139.35	116.38	376.04	288.30
Myo7a	1.83	2.71	5.48	1.35	3.02

Inflammatory Genes

Gene	A/J	BALB/c	B6	Long–Evans rat	Nile rat
Ifi44	12.90	5.50	0.60	3.77	2.82
Irf7	28.95	27.81	16.16	28.82	5.40
Stat1	14.06	10.56	10.35	19.27	11.22
Socs1	0.97	2.13	1.76	2.78	1.82

Long–Evans rat and Nile rat libraries were sequenced using paired–end sequencing using the Illumina GA IIX. Long–Evans rat data were aligned with University of California Santa Cruz rat genome assembly (rn4). Preliminary Nile rat data were assembled de novo by using Velvet and Oases software.

Materials

Immunohistochemistry:

Alexa 4, 6-diamidino-2-phenylindole (DAPI) and Alexa 488-conjugated peanut agglutinin (PNA) were purchased from Invitrogen. 1D4 (anti-rhodopsin mouse monoclonal antibody (mAb)) was a gift from Dr. Robert Molday (University of British Columbia). Rabbit anti-bone morphogenetic protein 4 (BMP4) polyclonal antibody (pAb), anti-mucolin 3 (MCOLN3) pAb, and anti-glutathione peroxidase 3 (GPX3) mAb were purchased from Abcam. Anti-cGMP phosphodiesterase 6C (PDE6C) pAb was purchased from Abgent. Anti-myosin 7a (MYO7A) mAb was obtained from the Developmental Studies Hybridoma Bank (University of Iowa). Rabbit anti-ionized calcium-binding adapter molecule 1 (Iba-1) pAb was provided by Wako. Rabbit anti-GFAP pAb was purchased from Dako. Cy3-conjugated goat anti-mouse IgG or goat anti-rabbit IgG (Promega) were used as secondary antibodies.

RT-PCR:

Probes used from Applied Biosystems were mouse *Gbp1* (Mm00657086_m1), *Gpx3* (Mm00492427_m1), *Irf7* (Mm00516788_m1), *Mcoln3* (Mm00460328_m1), *Myo7a* (Mm01274015_m1), *Opn1sw* (Mm00432058_m1), *Opn1mw* (Mm00433560_m1), *Rpe65* (Mm00504133_m1), *Stat1* (Mm00439531_m1), and *Tyro3* (Mm00444547_m1). The 18S rRNA (4319413E) probe set (Applied BioSystems) was used as the endogenous control.

References

1. Goc, A., Angel, T.E., Jastrzebska, B., Wang, B.L., Wintrobe, P.L., and Palczewski, K. 2008. Different Properties of the Native and Reconstituted Heterotrimeric G Protein Transducin. *Biochemistry* 47:12409-12419.
2. Golczak, M., Kiser, P.D., Lodowski, D.T., Maeda, A., and Palczewski, K. 2010. Importance of Membrane Structural Integrity for RPE65 Retinoid Isomerization Activity. *Journal of Biological Chemistry* 285:9667-9682.
3. Batten, M.L., Imanishi, Y., Maeda, T., Tu, D.C., Moise, A.R., Bronson, D., Possin, D., Van Gelder, R.N., Baehr, W., and Palczewski, K. 2004. Lecithin-retinol acyltransferase is essential for accumulation of all-trans-retinyl esters in the eye and in the liver. *Journal of Biological Chemistry* 279:10422-10432.